FISEVIER

Contents lists available at ScienceDirect

Acta Biomaterialia

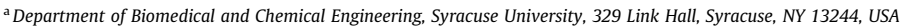
journal homepage: www.elsevier.com/locate/actabiomat



Full length article

Enzymatically triggered shape memory polymers

Shelby L. Buffington ^{a,b}, Justine E. Paul ^{a,1}, Matthew M. Ali ^{a,b,c,1}, Mark M. Macios ^a, Patrick T. Mather ^c, James H. Henderson ^{a,b,*}



^b Syracuse Biomaterials Institute, Syracuse University, 318 Bowne Hall, Syracuse, NY 13244, USA

ARTICLE INFO

Article history:
Received 31 August 2018
Received in revised form 8 November 2018
Accepted 20 November 2018
Available online 22 November 2018

Keywords: Stimuli responsive materials Enzyme responsive materials Shape memory polymers

ABSTRACT

Cytocompatible shape memory polymers activated by thermal or photothermal triggers have been developed and established as powerful "smart material" platforms for both basic and translational research. Shape memory polymers (SMPs) that could be triggered directly by biological activity have not, in contrast, been reported. The goal of this study was to develop an SMP that responds directly to enzymatic activity and can do so under isothermal cell culture conditions. To achieve this goal, we designed an SMP with a shape fixing component, $poly(\epsilon$ -caprolactone) (PCL), that is vulnerable to enzymatic degradation and a shape memory component, Pellethane, that is enzymatically stable - as the shape fixing component undergoes enzymatically-catalyzed degradation, the SMP returns to its original, programmed shape. We quantitatively and qualitatively analyzed material properties, shape memory performance, and cytocompatibility of the enzymatically-catalyzed shape memory response. The results demonstrate enzymatic recovery, as contraction of tensile specimens, using bulk enzymatic degradation experiments and show that shape recovery is achieved by degradation of the PCL shape-fixing phase. The results further showed that both the materials and the process of enzymatic shape recovery are cytocompatible. Thus, the SMP design reported here represents both an enzyme responsive material capable of applying a programmed shape change or direct mechanical force and an SMP that could respond directly to biological activity.

Statement of Significance

Cytocompatible shape memory polymers activated by thermal or photothermal triggers have become powerful "smart material" platforms for basic and translational research. Shape memory polymers that could be triggered directly by biological activity have not, in contrast, been reported. Here we report an enzymatically triggered shape memory polymer that changes its shape isothermally in response to enzymatic activity. We successfully demonstrate enzymatic recovery using bulk enzymatic degradation experiments and show that shape recovery is achieved by degradation of the shape-fixing phase. We further show that both the materials and the process of enzymatic shape recovery are cytocompatible. This new shape memory polymer design can be anticipated to enable new applications in basic and applied materials science as a stimulus responsive material.

© 2018 Acta Materialia Inc. Published by Elsevier Ltd. All rights reserved.

1. Introduction

Development of shape memory polymers possessing cytocompatible shape memory triggering mechanisms has led to increased application of these "smart" materials in both basic and transla-

tional research. SMPs memorize a permanent shape through chemical or physical cross-linking. Following manipulation and fixing in a temporary shape by an immobilizing transition, such as vitrification or crystallization, an SMP can subsequently recover to the permanent shape by a triggering event [1–4], such as thermal, electrical, or solvent activation [5–7]. Although biocompatible SMPs initially featured recovery temperatures too high for cells to maintain viability during the thermal trigger [8,9], in 2011 we [10–12] and then Ashby and colleagues [13] successfully applied

^c Department of Chemical Engineering, Bucknell University, 235 Dana Engineering Building, Lewisburg, PA 17837, USA

^{*} Corresponding author at: Syracuse Biomaterials Institute, 318 Bowne Hall, Syracuse University, Syracuse, NY 13244, USA.

E-mail address: jhhender@syr.edu (J.H. Henderson).

¹ These authors contributed equally to the current work.

SMPs as two-dimensional cell culture substrates with triggering of shape recovery at or near normal body temperature (37 °C). Subsequently, photothermally-triggered cytocompatible SMPs, activated by near-infrared wavelengths, were developed [14]. Two-dimensional SMP substrates and three-dimensional SMP scaffolds employing these cytocompatible triggering mechanisms have since been used in the study of mechanobiological aspects of cell morphology [15–19], cell differentiation [20–22], and cell motility [23,24], in the development of strategies for bone [25–33], cartilage [34] and nerve tissue engineering [35], and in the design of approaches for control of bacterial biofilms [36].

Enzymatically triggered, cytocompatible SMPs could open new fields of study and substantially broaden the range of existing basic and translational applications but have not previously been reported. If successfully achieved, enzymatic triggering of shape memory could enable, for example: drug delivery vehicles that affect the target cells/organs through controlled release that is modulated by the physiological status of the cells/organs; scaffolds that guide tissue regeneration through alterations in material and mechanical properties modulated by properties and behavior of the regenerating tissue; platforms for stem cell culture that present a tailored microenvironment to maintain stem cell phenotype or, alternatively, to differentiate cells down a specific lineage in response to the phenotypic state of the cells; and decisionmaking biosensors that use feedback systems to control patient treatment. Moreover, achievement of enzymatic triggering of shape memory would add to the growing field of enzymeresponsive materials, which currently includes materials based on material assembly or disassembly [37], coil-globule transitions [38], or degradation [39].

The goal of this study was to develop an SMP that responds directly to enzymatic activity and can do so under isothermal cell culture conditions. To achieve this goal, we designed an SMP with a shape fixing component that is vulnerable to enzymatic degradation and a shape memory component that is enzymatically stable—as the shape fixing component undergoes enzymatically-catalyzed degradation, the SMP returns to its original, programmed shape. We quantitatively and qualitatively analyzed material properties, shape memory performance, and cytocompatiblity of the enzymatically-catalyzed shape memory response.

2. Materials and methods

2.1. Study design

To develop an SMP that responds directly to enzymatic activity and can do so under cell culture conditions, we fabricated and characterized an SMP that combines an enzymatically labile fixing component, poly(ε-caprolactone) (PCL), with an enzymatically stable elastomer, Pellethane 5863-80A (hereafter, "Pellethane"; a polyether-based thermoplastic polyurethane elastomer) (Scheme 1). These two materials were selected so that, when heated above the T_m of PCL and then stretched and subsequently cooled, a temporary shape in which the PCL is under compression and the Pellethane under tension could be achieved. When later incubated in a solution of lipase—an enzyme produced by both eukaryotes and prokaryotes that hydrolyzes ester bonds in polyesters – the PCL would be degraded envzmatically, allowing the Pellethane to contract back to its original shape [40,41]. Fabrication was performed via dual-jet electrospinning [42-44]. Samples of varying %PCL content, referred to collectively hereafter as "fiber composites," were prepared to study the dependence of enzymatic recovery on sample composition. Two non-composite controls were used: samples containing only PCL (a control both for achievable shape fixing and for complete degradation in enzyme); and samples containing only Pellethane (a control both for lack of shape recovery and for lack of degradation in enzyme). Enzymatic shape recovery was studied using bulk degradation experiments in a lipase solution. Enzymatic recovery was quantitatively and qualitatively assessed via scanning electron microscopy (SEM), length measurements, and mass measurements. The cytocompatibility of the fiber composites and of the process of enzymatic recovery were assessed by respectively culturing of cells on samples without and with lipase present in the medium.

2.2. Materials

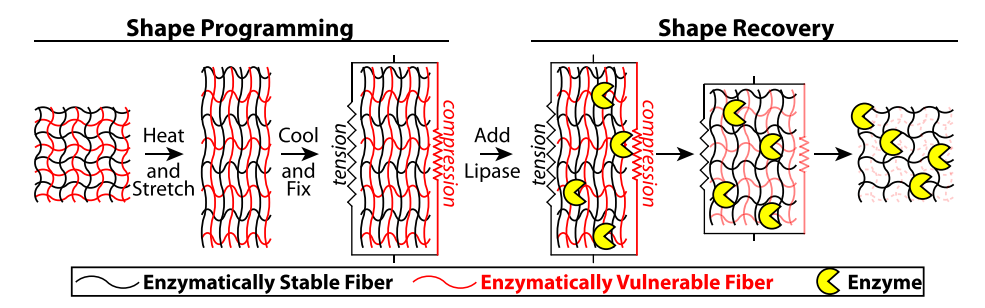
Pellethane® (5863-80A) pellets were kindly supplied by the Lubrizol Corporation. Poly(ϵ -caprolactone) (PCL) (Mn = 80,000 g/mol) pellets, chloroform (CHCl₃), N,N- dimethylformamide (DMF), and lipase derived from *Pseudomonas cepacia*, were purchased from Sigma-Aldrich. Tetrahydrofuran (THF) was purchased from VWR International. All materials were used as received. C3H/10 T1/2 cells (passage 8) were obtained from the American Type Culture Collection (ATCC) and expanded to passage 12–15 for experiments. Basal medium Eagle, fetal bovine serum, GlutaMAX, penicillin/streptomycin and LIVE/DEAD stain were all obtained from Invitrogen and used as received.

2.3. Fabrication

An 11 wt% electrospinning solution of Pellethane was prepared by dissolving 11 g of Pellethane in a 1:1.5 by volume solution of DMF:THF, as previously described [43]. A 15 wt% electrospinning solution of PCL was prepared by dissolving 15 g of PCL in a 1:4 by volume solution of DMF:CHCl₃. Solutions were stirred continuously for at least 24 h, at which time complete dissolution of the polymer was confirmed visually.

All samples were fabricated by dual electrospinning, in which two materials can be spun simultaneously to create a blended fiber mat (Schm. S1). Samples were electrospun using a custom electrospinning apparatus composed of a rotating cylindrical drum collector (95.6 mm diameter, 300 mm width). Spraybase[®] electrospinning syringe pumps, and Spraybase voltage sources with a multi-head emitter (Schm. S2). Two solution emitters, one for the Pellethane solution and one for the PCL solution, were used for this work. To vary the compositional ratio of the PCL to Pellethane in fiber composites, the flow rate of PCL was set between 2.02 and 8.07 mL/h, while the Pellethane flow rate was held constant at 11 mL/h, resulting in composites ranging from 20% to 50% PCL by mass. 22 G needles were attached to emitters and a voltage applied to the needle tip: 9-10.5 kV for the PCL, depending on the flow rate; and 12.5 kV for the Pellethane. The needle tip to mandrel distance was held constant at 148 mm for both emitters. A negative voltage of -1000 V was applied to the mandrel to improve fiber deposition. A rotational speed of 2000 rpm was used to align the fibers during electrospinning. To ensure uniform fiber deposition, the emitter needle tips were translated across the width of the mandrel following a square wave velocity profile with a peak velocity of 100 mm/s.

Non-composite PCL and Pellethane fiber mat controls were fabricated similarly, but using only one emitter. A flow rate of 8.07 mL/h with 10.5 kV was used for PCL and a flow rate of 11 mL/h with 12.5 kV was used for Pellethane. All other spin conditions were held constant. For enzymatic recovery experiments, because the PCL fiber mats (containing no Pellethane) were difficult to mechanically program, PCL controls were pressed in a hot press between two Teflon spacers at 70 °C to create a PCL film. In addition, the PCL present in fiber composites melts during heat treatment (Fig. S1, and described later in this section) and during programming; the resultant PCL film morphology present in fiber



Scheme 1. The strategy used to achieve enzymatic shape memory fiber composites. Fiber composites composed of $poly(\epsilon$ -caprolactone) (PCL) (red) and Pellethane (black) are heated and stretched above the T_m of PCL to program the samples. The composites are then cooled to fix the temporary shape, putting the Pellethane in an entropically unfavorable state. In this state, the Pellethane applies a compressive force to the PCL, as the Pellethane tries to recover back to its original shape but is resisted by the PCL crystallites that hold the temporary shape. Exposure to the enzyme lipase degrades the PCL portion of the fiber composite. As the PCL degrades, the force resisting the Pellethane is gradually removed and the Pellethane acts as an entropic spring to return back to its original conformation, recovering the permanent shape of the composite.

composites is similar to the PCL films prepared for the enzymatic recovery experiments. For assessment of cytocompatibility of material *prior* to enzymatic recovery, non-composite PCL fiber mats were washed in hexane and then cut in half. A portion of each fiber mat was compression molded (as above), and cell culture samples were cut from both the fiber mat and the film. We studied cytocompatibility of both the PCL fiber and film morphologies in the event that the mixed PCL fiber and film morphologies present in fiber composites differentially affected cells. For assessment of cytocompatibility of material *during* enzymatic shape recovery, of the PCL fiber and film samples, only the PCL film samples were studied, due to the difficulty in mechanically programming PCL fiber mats.

Thermal analysis (Section 2.4) was performed to measure the thermal degradation of the materials and to ensure that only fiber composites that had calculated composition values close to the prescribed values were used in subsequent experiments. Following thermal analysis, samples were heat treated, by heating the samples to 70 °C, to allow any residual strain programmed during the electrospinning process to recover [16]. Heat treatment was performed before dynamic mechanical analysis, shape memory testing, and enzymatic degradation experiments. For cytocompatibility experiments, samples were washed with hexane, to remove any residual toxic solvents that may have remained from electrospinning of the samples, and were then heat treated.

2.4. Thermal analysis

Thermal gravimetric analysis (TGA) (TA Instruments Q500) was performed on all fiber samples to measure the thermal degradation of the materials. To allow high-resolution analysis of thermal degradation events, the analysis employed a protocol in which samples are run at a variable heating rate that decreases as detected mass loss rate increases (TA Instruments Dynamic Rate Hi-Res^{$\rm IM$} Ramp). Briefly, and following methods we have previously reported [45], samples were heated at a maximum rate of 50 °C/min to 600 °C with a resolution of 4 °C and a sensitivity (instrument specific) of 1. When the instrument detected a thermal degradation, the heating rate automatically decreased (below 50 °C/min) to capture fully the degradation event, before continuing with the test.

Differential scanning calorimetry (DSC) (TA Instruments Q200) was performed on all samples using a DSC equipped with a refrigerated cooling system to record thermal transitions. For each test, samples weighing 3–5 mg were loaded into a T-zero aluminum plan and equilibrated by cooling to $-60\,^{\circ}\text{C}$. Samples were then heated at $10\,^{\circ}\text{C/min}$ to $170\,^{\circ}\text{C}$ and then immediately cooled at $5\,^{\circ}\text{C/min}$ to $-50\,^{\circ}\text{C}$. This initial heating and cooling cycle was used to erase any thermal history. Samples were then heated at

 $10\,^{\circ}\text{C/min}$ to $170\,^{\circ}\text{C}$ to measure the glass transition (T_g) and melting transition (T_m) of the fiber mats. The composition of each sample was calculated using the heat of crystallization of the PCL via Eq. (1) [46,47]. This equation assumes that the degree of crystallinity of the PCL phase is the same in all samples, which is reasonable because PCL readily crystallizes at room temperature. Calculated values were compared to predicted values prescribed by the flow rate of the PCL during electrospinning. Only fiber composites that had calculated composition values close to the prescribed values were used in subsequent experiments.

$$W_{PCL}(\%) = \frac{\Delta H_{PCL-COMP}}{\Delta H_{PCL-pure}} * 100$$
 (1)

Dynamic mechanical analysis (DMA) was used to measure the temperature dependences of the tensile storage modulus for all materials, as the temperature dependence of the storage modulus is a strong predictor of shape memory ability. Dog bones (ASTM D638 type IV, scaled down by a factor of 4) with a gauge length of 6.25 mm and width of 1.5 mm, were cut from fiber mats. Samples were then loaded into a DMA TA Q800, cooled to $-70\,^{\circ}\text{C}$, and then heated to 200 $^{\circ}\text{C}$ at a 2 $^{\circ}\text{C}/\text{min}$ while applying a small tensile deformation at a frequency of 1 Hz.

2.5. Shape memory ability

Thermal (not enzymatic) shape memory cycles were performed on a DMA (TA Instruments Q800) operated in controlled-force mode to quantify the shape memory ability of the fiber composites [48]. Briefly, each sample was first heated to 60 °C (above the $T_{\rm m}$ of PCL) and loaded at 0.03 N/min until 100% strain was reached. Samples were then cooled at 2 °C/min to 0 °C and the load released at 0.1 N/min. To complete the cycle, samples were then heated at 2 °C/min and the shape recovery recorded. This full cycle was repeated three times. The fixing (R_f) and recovery (R_r) ratios for each recovery event were then calculated using Eqs. (2) and (3), where shape "x" refers to the shape or deformation being programmed into the sample in the current cycle and shape "y" is the shape or deformation after the previous cycle [48].

$$Rf(x) = \frac{\varepsilon x}{\varepsilon x, load} \tag{2}$$

$$Rr(x \to y) = \frac{\varepsilon x - \varepsilon y, rec}{\varepsilon x - \varepsilon y}$$
 (3)

In Eq. (2), ε_x and $\varepsilon_{x,load}$ are, respectively, the strains measured after cooling and unloading (thus, the strain fixed) and before unloading (or the attempted programmed strain). $\varepsilon_{y,rec}$ is the strain achieved after recovery for shape y, and ε_y is the strain before programming shape y.

2.6. Enzymatic shape recovery experiments

Enzymatic shape recovery was assessed using bulk enzymatic degradation studies under simulated cell culture conditions. Samples were cut using a dog bone punch (the same punch used for DMA shape memory cycling), then heated and stretched to 100% strain using a custom screw-driven manual stretcher [49]. With samples so stretched but still in the stretching device, the stretcher and sample were transferred to a freezer at -20 °C to quickly fix the temporary shape (note: such fixing was stable at room temperature). Samples were photographed before and after mechanical programming (stretching and fixing) for subsequent use in image-based calculation of programmed strain and of strain during enzymatic shape recovery. Samples were then weighed and incubated in PBS solutions containing 0, 0.05, 0.1, or 0.5 mg/mL of lipase. The enzyme concentration range of 0.5-0.05 mg/mL was selected based on a previous experimental and kinetic modeling evaluation of lipase activity with respect to concentration for degradation experiments [40] and was chosen such that the highest enzyme concentration would ensure degradation of the PCL in a relatively short time frame (i.e., days) while the lower concentrations would reflect more physiological enzyme concentrations, though it is difficult to correlate in vitro concentration to activity in vivo. Experiments were conducted over 7 d, with one sample collected for analysis every 24 h. Experiments were repeated 3 times using fiber mats independently prepared (electrospun) on different days. Upon collection, the samples were washed using deionized water, dried in a desiccator for 24 h, and then transferred to a vacuum oven at 40 °C for 48 h to ensure full drying of the samples. Samples were then photographed and weighed. Mass loss was calculated using Eq. (4):

$$Mr(\%) = \frac{M(t)}{Mo} * 100$$
 (4)

where M_r is the % mass remaining, M(t) is the measured mass after degradation, and M_o is the original mass of the sample. To calculate programmed strain and strain during enzymatic shape recovery, images of samples before programming, after programming, and after sample collection were analyzed in ImageJ 1.51j8 (National Institutes of Health, Bethesda, MD, USA). In each image, a linear measurement of the gauge length was made along both sides of the dog bone samples. The two measurements were averaged. The measurements were performed independently by three separate users and averaged across all users. The change in strain (ε) over the course of enzymatic strain recovery for each sample was calculated using Eq. (5):

$$\Delta\varepsilon(\%) = \frac{(lo - ls)}{lo} * 100 \tag{5}$$

where $l_{\rm o}$ is the measured gauge length for the original, pre-strained sample and $l_{\rm s}$ is either the measured gauge length for the strained sample immediately after programming or after collection. DSC experiments were used to assess the PCL crystallinity before and after degradation. Samples were run hydrated immediately post degradation to better capture the crystallinity of PCL at the point of sample recovery.

2.7. SEM imaging

Fiber mats were imaged using SEM (JEOL 5600) to assess changes in fiber morphology during enzymatic shape recovery experiments and, additionally, to ensure that fiber morphologies were similar between fiber composite batches. Samples of fiber mats were collected for SEM immediately after electrospinning, immediately after the heat treatment used to recover residual strain programmed during the electrospinning process, and after

days 0 through 7 of the enzymatic shape recovery experiments. All samples were mounted on a metal plate and sputter coated for 45 s (Denton Vacuum-Desk II). Samples were imaged with an accelerating voltage of 10 kV and a spot size of 36.

2.8. Cell selection and expansion culture

All cell experiments were performed with the C3H/10 T1/2 mouse embryonic fibroblast line, a cell line we have frequently used in the development and application of cytocompatible SMPs [10,11,23]. Cells were obtained from the ATCC at passage 8, and cells of passage number 12–15 where used for experiments, following the recommendations of the ATCC. Cells were cultured in basal medium Eagle with 10% fetal bovine serum, 1% GlutaMAX, and 1% penicillin/streptomycin and passaged once 70–80% confluence was reached.

2.8.1. Cytocompatibility of material prior to enzymatic shape recovery Cells were directly cultured on samples to assess material cytocompatibility. Fiber and film PCL samples were sterilized using UV light for 10 h, flipped over, and sterilized using UV for an additional 10 h. All materials were soaked in complete medium overnight to allow proteins to adsorb throughout the samples and then C3H/10 T1/2 cells were solution seeded onto the materials at 10,000 cells/cm². Cell-seeded materials were then washed and stained with LIVE/DEAD at 24, 48, and 72 h time points with tissue culture polystyrene (TCPS) well plates acting as live controls for counting and analysis. Cell viability was calculated by dividing the total number of cells by the total number of live cells.

2.8.2. Cytocompatibility of material during enzymatic shape recovery

The cytocompatibility of enzymatic shape triggering was assessed by culturing cells on samples as the samples were incubated in lipase-containing medium over a one-week period. Samples were washed and sterilized as described in Section 2.8.2. Cells were seeded onto the samples at 5000 cells/cm² and allowed to attach for 3 h. The culture medium was then replaced with medium containing 0.5 mg/mL lipase, the highest lipase concentration used for shape recovery experiments. The lipase-containing medium was sterilized via filtration with a 0.45 µm filter prior to use. The non-toxic control was lipase-free medium. Media were changed every 2 days to mimic conditions used in the bulk degradation experiments. Samples were collected and cells stained with LIVE/DEAD stain at 1, 3, and 7 day time-points to assess cell viability. Cell viability was calculated as above (Section 2.8.2).

2.9. Statistical methods

For numerical graphs, error bars show the sample standard deviation. Statistical analysis was performed using RStudio Version 1.1.453 (The R Foundation for Statistical Computing) and comparisons were made using a multiple comparison Holm t test. Significance was set at P < 0.05. For enzymatic shape recovery (Section 3.3), PCL samples were excluded from comparisons as samples at some time points were completely degraded.

3. Results

3.1. Thermal analysis

As anticipated, thermal transitions quantified by TGA (Fig. S2, Table S1), DSC (Fig. 1), and DMA (Fig. S3) showed that both PCL and Pellethane were present in fiber composites and existed as separate phases, as evidenced by the separate transitions recorded in thermal analysis. TGA analysis (Fig. S2) showed that all fiber

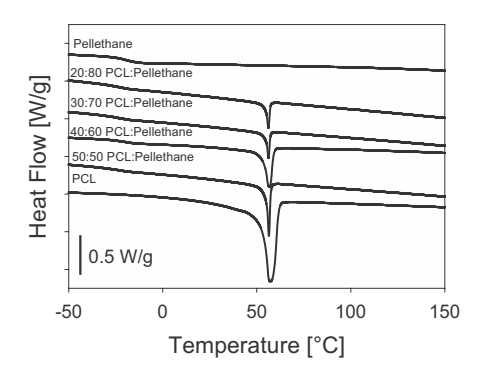


Fig. 1. Differential scanning calorimetry (DSC) thermograms of all dual spun materials ordered in order of increasing poly(ε-caprolactone) (PCL) content. Increasing PCL content resulted in a large exotherm for the PCL melt transition but did not result in shifting of the T_m of PCL. This exotherm at approximately 56 °C was used to calculate the predicted incorporation of PCL during the electrospinning process, and only fiber mats within 5% of the predicted PCL content were used in subsequent experiments. DSC traces are in order of increasing PCL content, from top to bottom: Pellethane, 20:80 PCL:Pellethane, 30:70 PCL:Pellethane, 40:60 PCL: Pellethane, 50:50 PCL:Pellethane, and PCL.

mats were dry before processing. PCL showed a single sharp degradation event, while Pellethane showed a two-step degradation event. Fiber composites likewise showed a two-step degradation; however, the degradation of the PCL was occluded by the degradation of the Pellethane, making TGA analysis of the two weight %s difficult. As a result, DSC was used to analyze the % content of the fiber mats. For the analyzed temperature range, Pellethane controls demonstrated only a $T_{\rm m}$, at approximately $-20\,^{\circ}\text{C}$, while PCL controls showed only a $T_{\rm m}$, at approximately $56\,^{\circ}\text{C}$ (Table S1). To ensure consistency across experimental runs, only fiber composites that came within a $\pm5\%$ predicted PCL content were used for subsequent experiments. Analysis of post-heat treatment samples confirmed that the thermal transitions quantified by TGA and DSC were unaffected by the heat treatment used to recover residual strain programmed during the electrospinning process (data not shown).

DMA showed three well-separated thermal-mechanical transitions at approximately $-20\,^{\circ}\text{C}$, $56\,^{\circ}\text{C}$, and $160\,^{\circ}\text{C}$ for the T_g of the Pellethane, the T_m of the PCL, and the T_m of the Pellethane, respectively (Fig. S3). For our approach to achieving enzymatic shape memory, the ideal point for shape memory behavior would be above the T_g of Pellethane, so the material is within its elastic region, with the T_m of PCL acting as the triggering temperature.

3.2. Shape memory ability

Thermal shape memory cycles demonstrated that strong shape fixing and recovery were achieved for fiber composite samples (Fig. 2). The PCL control yielded during the first stretch of the first cycle and was not included in analysis. The Pellethane control (Fig. 2A) showed a poor fixing ratio of 53%, indicating a low ability to fix a shape, and demonstrated a recovery ratio of 89%. We note, for comparison, that an ideal rubber features no (0%) fixing and complete (100%) recovery. The high recovery ratio for the Pellethane control is attributed to the elasticity of the Pellethane fibers, which is the driving force for shape recovery. This recovery ratio indicates that some strain is lost during mechanical cycling, which we attribute to minor plastic deformation that occurs during the first thermo-mechanical cycle. The fixing ratio of fiber composites was 89% and 96% for the 20:80 (Fig. 2B) and 50:50 (Fig. 2C) PCL:Pellethane, respectively (Summarized in Table S2), indicating that increasing the PCL content increased the fixing ability of the fibers. The recovery ratio showed weak dependence on composition, with values of 89% and 84% for the 20:80 (Fig. 2B) and 50:50 (Fig. 2C) PCL:Pellethane, respectively (Summarized in Table S3). The 30:70 and 40:60 PCL:Pellethane compositions showed similar results, with an increase in PCL content increasing the fixing ability of the fibers and the recovery ratio showing weak dependence on composition (Fig. S4). All samples showed a diminished recovery ratio for the first cycle, which we attribute to minor plastic deformation of the Pellethane fibers, as indicated by the strain in the samples not returning fully to zero. After a single mechanical conditioning step, the recovery of the materials increased. In light of the modest differences in shape memory ability observed across the four fiber composite compositions tested, only the two most extreme compositions, 20:80 and 50:50 PCL: Pellethane, were studied in the ensuing enzymatic shape recovery and cytocompatibility experiments.

3.3. Enzymatic shape recovery

Enzyme-triggered shape recovery was observed in fiber composites (50:50 and 20:80 PCL:Pellethane, Figs. 3 and 4 and S5), as evidenced by decreasing strain over the 7-day experiment. However, shape recovery was only evident for the highest enzyme concentration studied (0.5 mg/mL). Pellethane showed no measurable changes in strain for all conditions, as expected, while the fiber composites decreased in length over time (Fig. 4A). Lower concentrations of lipase degraded the PCL film control samples but did not

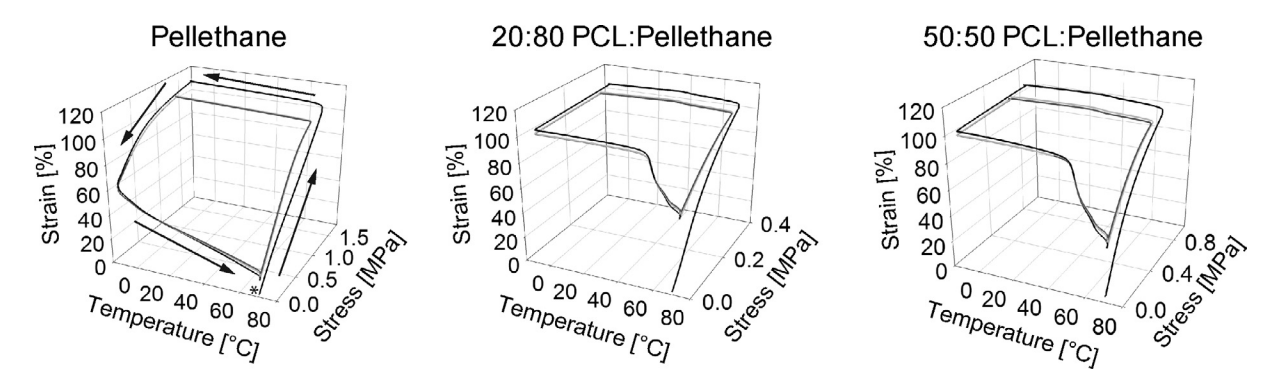


Fig. 2. Thermal shape memory cycles. A) Pure Pellethane showed a fixing ratio (R_f) of 54% and a recovery ratio (R_r) of 87%. B) The 20:80 PCL:Pellethane fiber composite showed an R_f of 93.5% and an R_r of 85.1%. C) The 50:50 PCL:Pellethane fiber composite showed an R_f of 97.5% and an R_r of 83.2%. One shape memory cycle comprises the following steps: starting at the asterisk, the sample is heated to 60 °C, and then the force is ramped to stretch the sample; the sample is then cooled to 0 °C and unloaded; the sample is then heated back to 60 °C to measure recovery. This cycle was completed three times with cycles 1, 2, and 3 shown in black, light gray, and dark gray, respectively. (For interpretation of the references to color in this figure legend, the reader is referred to the web version of this article.)

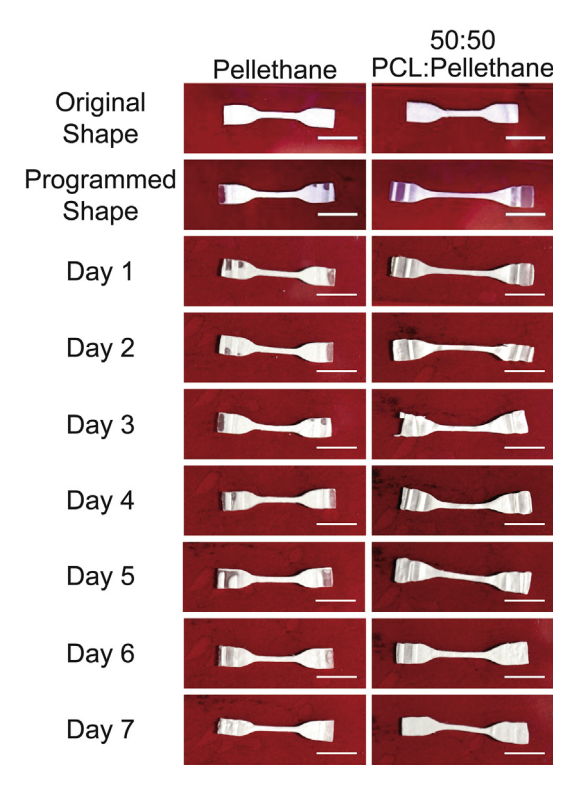


Fig. 3. Macroscopic view of enzymatic recovery. Pictures of samples were taken before and after programming and after being exposed to 0.5 mg/mL lipase solution over the course of 7 days. Pellethane controls (left) and 50:50 PCL:Pellethane fiber composites (right) are shown. After programming, the Pellethane showed no shape fixing and no measured change in length over the 7-day incubation. In contrast, the 50:50 PCL:Pellethane fixed a temporary shape and then contracted over the course of 7 days. Scale bar is 1 cm. Results for 20:80 PCL:Pellethane and for the PCL controls are available in Fig. S5.

trigger shape recovery in the fiber composites (Fig. 4B and C). For fiber composites, sample lengths (and associated strains) in 0.5 mg/mL lipase solutions (Fig. 4A) remained significantly greater (P < 0.05) than the Pellethane controls until day 5, after which no statistical difference in length was observed, consistent with samples having recovered to the preferred length of the Pellethane. In contrast, when incubated in 0.1 (Fig. 4B) and 0.05 mg/mL (Fig. 4C) lipase, fiber composite sample lengths remained significantly greater than that of the Pellethane controls at all time-points (P < 0.05), consistent with fiber composite samples having not recovered. Further, PBS controls showed no measurable recovery for all groups, as anticipated (Fig. 4D). In particular, those samples incubated in only PBS exhibited no measurable change in strain with time, remaining strained at the magnitude programmed, which was significantly greater than that of Pellethane control (incapable of strain-fixing), for all time points (P < 0.05). PCL control samples were not included in statistical comparisons, as samples degraded significantly for all enzyme concentrations, including day 1.

Mass change measurements revealed significant mass loss for the PCL film, with rate of degradation increasing with increasing lipase concentration, while all other samples exhibited no measurable mass loss (Fig. 5). Control samples immersed in PBS showed no measurable mass change for any of the samples (Fig. 5D), indicating that mass loss was driven by enzymatic degradation instead of much slower hydrolytic degradation, as expected. The lack of observed mass change in fiber composites (Fig. 5) suggests that the observed strain recovery (Fig. 4) occurs primarily through reduction of PCL molecular weight, or disruption of the percolation of the PCL phase, not through loss of PCL mass. This finding is supported by the observed decrease in PCL crystallinity as samples are degraded (Fig S6). Upon exposure to lipase the PCL crystalline peak diminishes supporting the degradation disrupting the PCL crystallinity and thereby allowing the Pellethane to recover.

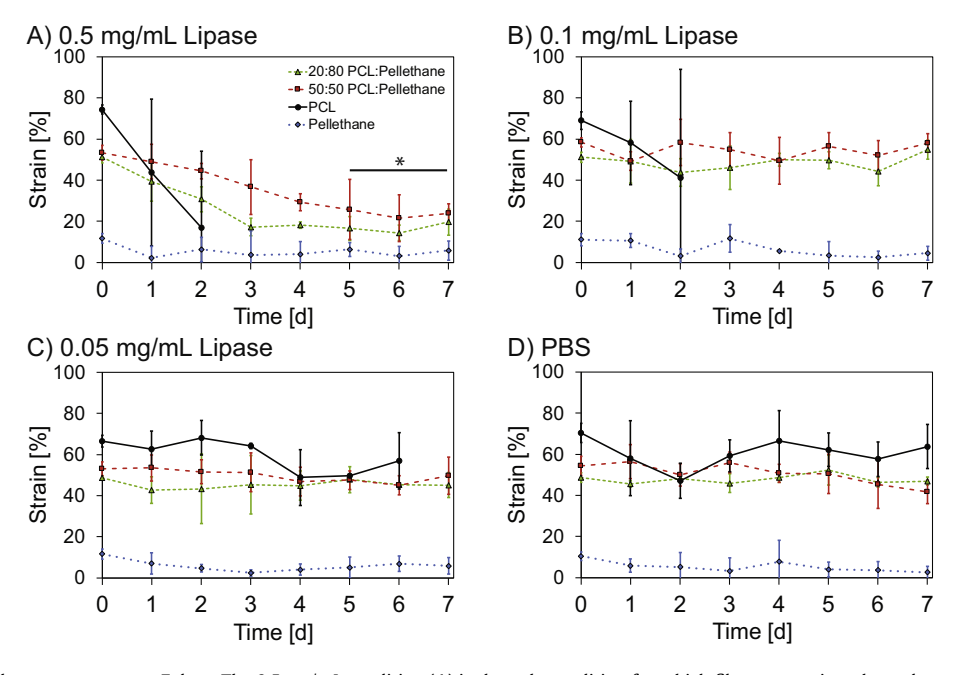


Fig. 4. Enzyme-triggered shape recovery over 7 days. The 0.5 mg/mL condition (A) is the only condition for which fiber composites showed measurable, significant sample recovery. The 0.1 mg/mL (B) and 0.05 mg/mL (C) conditions showed no measurable sample recovery. The PBS control (D) showed no strain changes for any groups, including the PCL control, over the course of the 7-day experiment. For all conditions, the fiber composites (20:80 and 50:50 PCL:Pellethane) showed a significantly different length compared to Pellethane controls, except for days 5–7 in the 0.5 mg/mL condition. * and bar indicate the three time points for which the strain of fiber composites was no longer statistically different from that of the Pellethane controls (P > 0.05), indicating sample recovery. For all groups, the value at day 0 is the mean programmed strain of all 21 samples (3 replicates × 7 time points), and the value at each subsequent time point is the mean of the 3 samples collected at that time point.

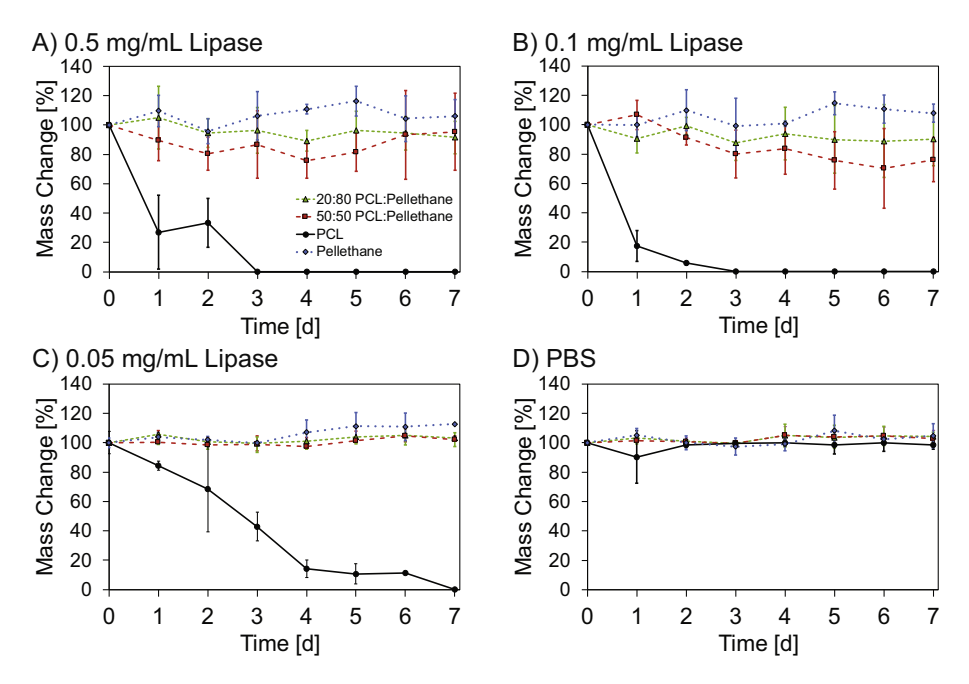


Fig. 5. Mass change during degradation. Significant mass loss was observed for the PCL film in all conditions: (A) 0.5 mg/mL lipase; (B) 0.1 mg/mL lipase; (C) 0.05 mg/mL lipase; and (D) PBS (0 mg/mL lipase)). All other samples exhibited no measurable mass loss.

Morphological analysis by SEM of samples undergoing degradation during exposure to enzyme revealed changes in sample morphology indicative of PCL degradation. Surface analysis of morphological changes in the 50:50 PCL:Pellethane fiber composite incubated in 0.5 mg/mL lipase (Fig. 6) showed an initial (predegradation) morphology of fibers with a film or binder at the surface (Fig. 6A). Over the course of the degradation experiment, the morphology of the fiber composite transitioned from a mixed film-fiber morphology (Fig. 6A-C) to a predominantly fiber morphology (Fig. 6D) as PCL degraded, leaving behind primarily Pellethane fibers. Analysis of cross-sections of 50:50 PCL:Pellethane samples (Fig. 6E) showed an initial semi-continuous network of Pellethane fibers interpenetrated incompletely by PCL binder, with significant porosity evident. As enzymatic degradation progressed over 7 days, the PCL binder increasingly degraded until, at day 7 (Fig. 6H), the fraction of PCL had diminished substantially. The 20:80 PCL:Pellethane samples showed similar morphological changes when incubated in 0.5 mg/mL lipase (Fig. S9B), and both fiber composites (20:80 and 50:50) also showed similar morphological changes when incubated in the lower, 0.1 mg/mL, lipase concentration (Fig. S8B and C). In contrast, fiber composites incubated in 0.05 mg/mL lipase retained a mixed film-fiber morphology (Fig. S7B and C). The Pellethane control showed no morphological changes, regardless of enzyme concentration (Figs. S7A, S8A, S9A, S10A). All fiber composites and controls showed no morphological changes when incubated in PBS (Fig. S7).

3.4. Cytocompatiblity of materials prior to enzymatic shape recovery

When mouse fibroblasts were cultured directly on fiber composites and non-composite controls in the absence of lipase, no statistically significant differences in viability were found (Fig. 7). Moreover, all groups had a viability of 75% or greater at all timepoints. The Pellethane control, PCL control, and fiber composites showed an average viability not statistically different from the TCPS control, indicative of cytocompatibility (representative cell

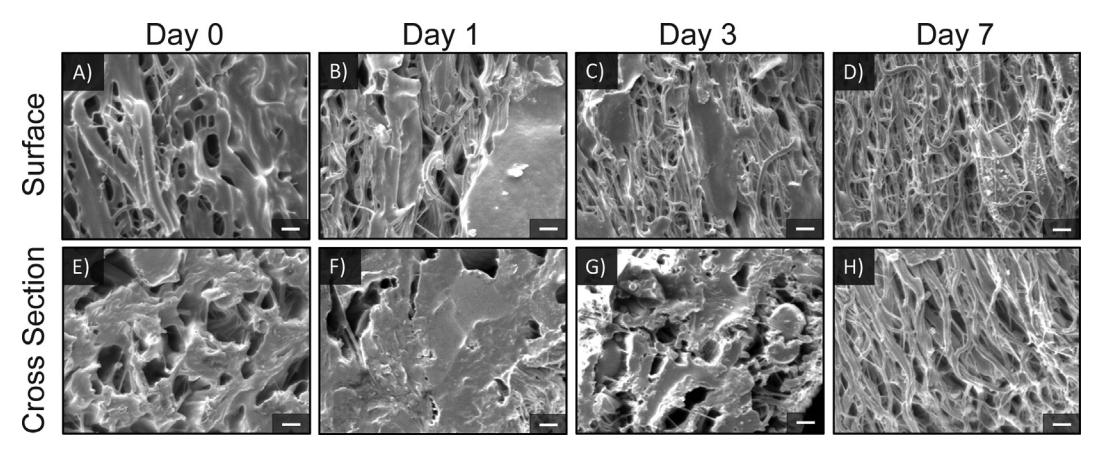


Fig. 6. SEM micrographs of 50:50 PCL:Pellethane incubated in 0.5 mg/mL of lipase. Morphological analysis shows changes in sample morphology indicative of PCL degradation (A–D) at the surface and (E–H) in cross-section of 50:50 PCL:Pellethane fiber composites for day 0, 1, 3, 7, respectively. Day 0 shows the 50:50 fiber composite after heat treatment but before any strain programming or enzymatic recovery. Scale bar is 10 μm. Results for both fiber composites (20:80 and 50:50 PCL:Pellethane) and for the PCL controls under all incubation conditions (0.5 mg/mL, 0.1 mg/mL, and 0.05 mg/mL lipase and PBS) are available in Figs. S6 through S9).

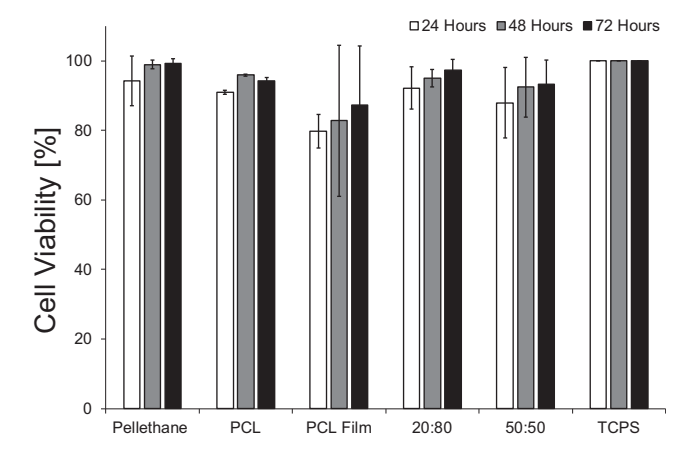


Fig. 7. Cell viability of C3H/10 T1/2 cells cultured directly on fiber composite and non-composite control samples in the absence of lipase. No significant differences were found between any groups (P > 0.05), and viability was >75% for all groups. Groups are Pellethane control, PCL control, compressed PCL Film control, 20:80 PCL: Pellethane fiber composite, 50:50 PCL:Pellethane fiber composite, and tissue culture polystyrene control.

images for all groups are shown in Fig. S10). Qualitatively, cells cultured on the 50:50 PCL:Pellethane fibrous composite showed a random orientation that contrasted with that of cells cultured on the Pellethane control, which showed an oriented morphology (Fig. S11). This difference is likely due to the morphology of the PCL, which acts as a film (binder) in the fiber composites (Figs. 6, S1), a morphological feature that does not exist between the aligned fibers of the Pellethane control. Image analysis revealed a significantly higher number of cells on TCPS compared to all material groups (Fig. S12, P < 0.05), likely due to cells attaching to the bottom of the well (rather than the sample) during the seeding of material groups.

3.4.1. Cytocompatibility of material during enzymatic shape recovery When mouse fibroblasts were cultured on fiber composites and non-composite controls incubated with 0.5 mg/mL of lipase or a lipase-free control medium (Fig. 8), no statistical differences in viability were found. Moreover, all groups had a viability of 75% or greater at all time-points. As had been observed in the study of cytocompatibility prior to enzymatic shape recovery (Fig. 7), in

the presence of lipase the Pellethane control, PCL control, and fiber composites showed an average viability not statistically different from the TCPS control, indicative of the enzymatic degradation of PCL and, therefore, the phenomenon of enzymatic shape recovery being cytocompatible (Fig. 8, and representative cell images for all groups are shown in Figs. S13 and S14). Image analysis again revealed a significantly higher number of cells on TCPS compared to all material groups (Fig. S15, P < 0.05), which is again likely due to cells attaching to the bottom of the well (rather than the sample) during the seeding of material groups.

4. Discussion

Here we have introduced and studied a new SMP design that responds directly to enzymatic activity to allow isothermal shape change, demonstrated as contraction of tensile specimens, under cell culture conditions. Electrospun fiber composites prepared using this design showed good thermal shape memory ability, with a PCL component acting as a shape fixer and a Pellethane component acting as the memory component. When cultured in a 0.5 mg/mL lipase solution, programmed fiber composites showed enzymatic shape recovery within a 7-day test period. Cells cultured on enzymatic SMPs with or without 0.5 mg/mL lipase showed viability comparable to non-toxic controls, indicating that both the enzymatically-responsive SMP materials and the process of enzymatic shape recovery are cytocompatible.

The enzymatic shape recovery achieved in the present work is dependent on enzyme concentration. Only samples incubated in the highest enzyme concentration, 0.5 mg/mL lipase, showed complete shape recovery, while samples incubated in lower enzyme concentrations and in a lipase-free control showed no measurable recovery. This enzyme concentration sensitivity is consistent with the strategy used to achieve enzymatic recovery (Scheme 1), wherein shape recovery is enabled by the degradation of an enzymatically labile fixing component and is only achieved when that component has degraded sufficiently. It is expected that, if degradation experiments were lengthened, all fiber composites would eventually show full strain recovery for all enzyme conditions studied.

The enzymatic SMPs did not demonstrate mass loss during recovery. This finding suggests that the mechanism of enzyme shape recovery is either a decrease in PCL molecular weight or de-percolation of the fixing phase. As either of these processes

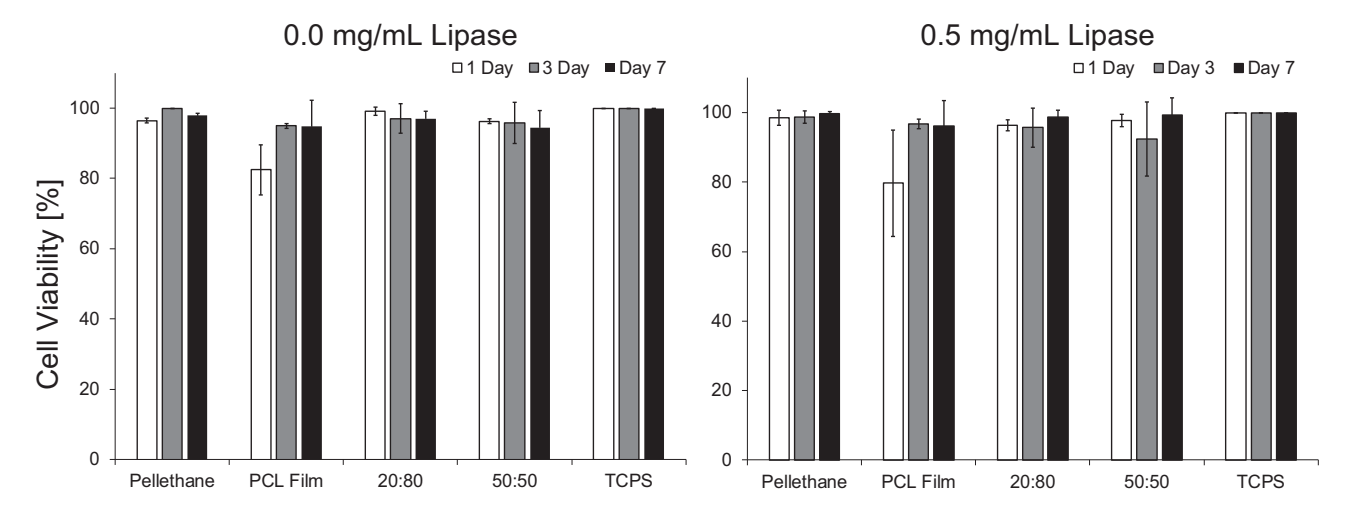


Fig. 8. Cell viability of C3H/10 T1/2 cells cultured directly on fiber composite and non-composite control samples in (left) a lipase-free control medium or (right) the presence of 0.5 mg/mL lipase. No significant differences were found between any groups (P > 0.05), and viability was >75% for all groups. Groups are Pellethane control, compressed PCL Film control, 20:80 PCL:Pellethane fiber composite, 50:50 PCL:Pellethane fiber composite, and tissue culture polystyrene control.

continue, the force exerted by the Pellethane is able to overcome the force exerted by the PCL, leading to recovery back to the sample's original shape. Analysis of SEM micrographs suggests that the PCL phase is in fact degrading, lending support to the hypothesized de-percolation of PCL. This theory is supported by the observed decrease in the heat of crystallization of PCL over time, a decrease from 9.031 to 0 W/g over 7 days for the 50:50 PCL:Pellethane fiber composite (Fig. S6). In addition, the PCL control samples degrade within 2 days, compared to the 5 days required to observe sample recovery in the programmed fiber composites. These findings suggest that the presence of Pellethane in the composite samples inhibits the ability of the lipase to diffuse into the fiber composites and degrade the PCL shape fixing component and, further, that the mechanism of degradation is not mass loss but loss of crystallinity and concomitant softening of the PCL-based fixing phase.

A potential limitation of this first instantiation of the new SMP design is the relatively long time and high enzyme concentration required for enzymatic shape recovery. Few cell types may release enzyme at concentrations necessary for enzymatic shape recovery to occur in time-spans less than weeks or months. Because we speculate that the present material composition would recover in low enzyme concentrations, but over long time periods, the present composition may be best suited for applications in which slow response is beneficial or for applications in which cells, such as macrophages or hepatic cells [50,51], secrete high concentrations of enzyme. It is anticipated that the new SMP design could be adapted for more rapid recovery and/or low enzyme concentration triggering by increasing the enzymatic sensitivity of the labile fixing component. Conversely, even more gradual recovery than that demonstrated here could be achieved by decreasing enzymatic sensitivity of the labile fixing component. More generally, enzymatically responsive SMPs could, in theory, be designed to be triggered by any arbitrary enzyme by engineering the enzyme's target sequence into the polymer, though risk of cytotoxicity would likely be a constraint for many candidate enzymes.

In addition to contributing to SMP science, the new design reported here adds SMPs to the field of enzyme responsive materials (ERMs) – materials that undergo a material action, such as self-assembly/disassembly [37], transformation of surface properties, or swelling/deswelling [38], in response to enzymatic activity. ERMs have gained increasing attention due to the extreme specificity with which they can be designed to respond to the biological environment. For example, Zelzer and colleagues [52] developed an ERM that changes surface properties in response to dephosphorylation, with sensitivity sufficient for cells to provide the trigger. Liu and colleagues [53] designed enzymatically stiffening hydrogels to study how cancer cells modify their behavior in response to stiffening gels. Despite advances, such as these, in ERM science, prior to the present work there was not an ERM capable of applying a programmed shape change or direct mechanical force.

In addition to bringing shape-changing functionality to the field of ERMs, the SMP design reported here represents the first SMP that could respond directly to biological activity. The majority of cell culture compatible SMPs have been thermally or photothermally triggered. Dependence on these triggers prevents application as stimuli responsive materials designed to respond directly to biological activity [54]. With the advent of enzymatically triggered SMPs, SMPs can now be designed for such application.

5. Conclusion

We have developed an enzymatically triggered SMP that changes its shape isothermally in response to enzymatic activity under cell culture conditions. We successfully demonstrated enzymatic recovery using bulk enzymatic degradation experiments. The results show that shape recovery is achieved by degradation

of the PCL shape-fixing phase, which enables one-way and onetime shape recovery, leaving the material in a final state that, while useful in itself, does not allow for reprogramming. We further showed that both the materials and the process of enzymatic shape recovery are cytocompatible. This new SMP design can be anticipated to enable new applications in basic and applied materials science as a stimulus responsive material.

Acknowledgements

Funding from the NSF IGERT Program, DGE-1068780, and the NSF BMAT program, DMR-1609523 and REU Supplement DMR-1743080, is gratefully acknowledged, as is use of the facilities of the Syracuse Biomaterial Institute at Syracuse University.

Conflict of interest

The authors confirm that there are no known conflicts of interest associated with this publication and there has been no significant financial support for this work that could have influenced its outcome.

Data availability

The raw/processed data required to reproduce these findings cannot be shared at this time due to technical or time limitations, but they can be provided upon requested.

Appendix A. Supplementary data

Supplementary data to this article can be found online at https://doi.org/10.1016/j.actbio.2018.11.031.

References

- [1] M.D. Hager, S. Bode, C. Weber, U.S. Schubert, Shape memory polymers: Past, present and future developments, Prog. Polym. Sci. 49–50 (2015) 3–33, https://doi.org/10.1016/j.progpolymsci.2015.04.002.
- [2] C. Liu, H. Qin, P.T. Mather, Review of progress in shape-memory polymers, J. Mater. Chem. 17 (2007) 1543, https://doi.org/10.1039/b615954k.
- [3] H. Meng, G. Li, A review of stimuli-responsive shape memory polymer composites, Polym. (United Kingdom) 54 (2013) 2199–2221, https://doi.org/ 10.1016/j.polymer.2013.02.023.
- [4] A. Lendlein, S. Kelch, Shape-memory polymers, Angew. Chemie Int. Ed. 41 (2002) 2034, https://doi.org/10.1002/1521-3773(20020617)41:12<2034::AID-ANIE2034>3.0.CO;2-M.
- [5] X. Luo, P.T. Mather, Conductive shape memory nanocomposites for high speed electrical actuation, (n.d.). doi:10.1039/c001295e.
- [6] X. Gu, P.T. Mather, Water-triggered shape memory of multiblock thermoplastic polyurethanes, TPUs3 3 (2013), https://doi.org/10.1039/c3ra41337c.
- [7] J. Mendez, P.K. Annamalai, S.J. Eichhorn, R. Rusli, S.J. Rowan, E.J. Foster, C. Weder, Bioinspired mechanically adaptive polymer nanocomposites with water-activated shape-memory effect, Macromolecules 44 (2011) 6827–6835, https://doi.org/10.1021/ma201502k.
- [8] A. Lendlein, M. Behl, B. Hiebl, C. Wischke, Shape-memory polymers as a technology platform for biomedical applications, Expert Rev. Med. Devices 7 (2010) 357–379, https://doi.org/10.1586/erd.10.8.
- [9] S. Neuss, I. Blomenkamp, R. Stainforth, D. Boltersdorf, M. Jansen, N. Butz, A. Perez-Bouza, R. Knüchel, The use of a shape-memory poly(ε-caprolactone) dimethacrylate network as a tissue engineering scaffold, Biomaterials 30 (2009) 1697–1705, https://doi.org/10.1016/J.BIOMATERIALS.2008.12.027.
- [10] K.A. Davis, K.A. Burke, P.T. Mather, J.H. Henderson, Dynamic cell behavior on shape memory polymer substrates, Biomaterials 32 (2011) 2285–2293, https://doi.org/10.1016/j.biomaterials.2010.12.006.
- [11] K.A. Davis, X. Luo, P.T. Mather, J.H. Henderson, Shape memory polymers for active cell culture, J. Vis. Exp. (2011) e2903, https://doi.org/10.3791/2903.
- [12] X. Xu, K.A. Davis, P. Yang, X. Gu, J.H. Henderson, P.T. Mather, Shape memory RGD-containing networks: synthesis, characterization, and application in cell culture, Macromol. Symp. 309–310 (2011) 162–172, https://doi.org/ 10.1002/masy.201100060.
- [13] D.M. Le, K. Kulangara, A.F. Adler, K.W. Leong, V.S. Ashby, Dynamic topographical control of mesenchymal stem cells by culture on responsive Poly(∈-caprolactone) surfaces, Adv. Mater. 23 (2011) 3278–3283, https://doi.org/10.1002/adma.201100821.

- [14] Q. Shou, K. Uto, W.C. Lin, T. Aoyagi, M. Ebara, Near-infrared-irradiation-induced remote activation of surface shape-memory to direct cell orientations, Macromol. Chem. Phys. 215 (2014) 2473–2481, https://doi.org/10.1002/macp.201400353.
- [15] P. Yang, R.M. Baker, J.H. Henderson, P.T. Mather, V.S. Ashby, N. Butz, A. Perez-Bouza, R. Knuchel, M. Khine, In vitro wrinkle formation via shape memory dynamically aligns adherent cells, Soft Matter 9 (2013) 4705, https://doi.org/10.1039/c3sm00024a.
- [16] L.-F. Tseng, P.T. Mather, J.H. Henderson, Shape-memory-actuated change in scaffold fiber alignment directs stem cell morphology, Acta Biomater. 9 (2013) 8790–8801, https://doi.org/10.1016/j.actbio.2013.06.043.
- [17] M. Ebara, M. Akimoto, K. Uto, K. Shiba, G. Yoshikawa, T. Aoyagi, Focus on the interlude between topographic transition and cell response on shape-memory surfaces, Polymer (Guildf). 55 (2014) 5961–5968, https://doi.org/10.1016/J. POLYMER.2014.09.009.
- [18] P.Y. Mengsteab, K. Uto, A.S.T. Smith, S. Frankel, E. Fisher, Z. Nawas, J. Macadangdang, M. Ebara, D.-H. Kim, Spatiotemporal control of cardiac anisotropy using dynamic nanotopographic cues, Biomaterials 86 (2016) 1–10, https://doi.org/10.1016/J.BIOMATERIALS.2016.01.062.
- [19] M. Ebara, K. Uto, N. Idota, J.M. Hoffman, T. Aoyagi, Shape-memory surface with dynamically tunable nano-geometry activated by body heat, Adv. Mater. 24 (2012) 273–278, https://doi.org/10.1002/adma.201102181.
- [20] E.M. Lee, K. Smith, K. Gall, B.D. Boyan, Z. Schwartz, Change in surface roughness by dynamic shape-memory acrylate networks enhances osteoblast differentiation, Biomaterials 110 (2016) 34–44, https://doi.org/10.1016/J. BIOMATERIALS.2016.08.004.
- [21] T. Gong, K. Zhao, G. Yang, J. Li, H. Chen, Y. Chen, S. Zhou, The control of mesenchymal stem cell differentiation using dynamically tunable surface microgrooves, Adv. Healthc. Mater. 3 (2014) 1608–1619, https://doi.org/ 10.1002/adhm.201300692.
- [22] L.-F. Tseng, J. Wang, R.M. Baker, G. Wang, P.T. Mather, J.H. Henderson, Osteogenic capacity of human adipose-derived stem cells is preserved following triggering of shape memory scaffolds, Tissue Eng. Part A 22 (2016) 1026–1035, https://doi.org/10.1089/ten.tea.2016.0095.
- [23] R.M. Baker, M.E. Brasch, M.L. Manning, J.H. Henderson, Automated contour-based tracking and analysis of cell behaviour over long time scales in environments of varying complexity and cell density, J. R. Soc. Interface 11 (2014), https://doi.org/10.1098/rsif.2014.0386. 20140386.
- [24] J. Wang, A. Quach, M.E. Brasch, C.E. Turner, J.H. Henderson, On-command on/off switching of progenitor cell and cancer cell polarized motility and aligned morphology via a cytocompatible shape memory polymer scaffold, Biomaterials 140 (2017) 150–161, https://doi.org/10.1016/J.BIOMATERIALS.2017.06.016.
- [25] J. Wang, M.E. Brasch, R.M. Baker, L.-F. Tseng, A.N. Peña, J.H. Henderson, Shape memory activation can affect cell seeding of shape memory polymer scaffolds designed for tissue engineering and regenerative medicine, J. Mater. Sci. Mater. Med. 28 (2017) 151, https://doi.org/10.1007/s10856-017-5962-z.
- [26] R.M. Baker, L.-F. Tseng, M.T. Iannolo, M.E. Oest, J.H. Henderson, Self-deploying shape memory polymer scaffolds for grafting and stabilizing complex bone defects: a mouse femoral segmental defect study, Biomaterials 76 (2016) 388– 398, https://doi.org/10.1016/J.BIOMATERIALS.2015.10.064.
- [27] R.M. Baker, J.H. Henderson, P.T. Mather, Shape memory poly(ε-caprolactone)-co-poly(ethylene glycol) foams with body temperature triggering and two-way actuation, J. Mater. Chem. B. 1 (2013) 4916, https://doi.org/10.1039/c3tb20810a.
- [28] B. Zhang, T.M. Filion, A.B. Kutikov, J. Song, Facile stem cell delivery to bone grafts enabled by smart shape recovery and stiffening of degradable synthetic periosteal membranes, Adv. Funct. Mater. 27 (2017) 1604784, https://doi.org/ 10.1002/adfm.201604784.
- [29] P. Rychter, E. Pamula, A. Orchel, U. Posadowska, M. Krok-Borkowicz, A. Kaps, N. Smigiel-Gac, A. Smola, J. Kasperczyk, W. Prochwicz, P. Dobrzynski, Scaffolds with shape memory behavior for the treatment of large bone defects, J. Biomed. Mater. Res. Part A. 103 (2015) 3503–3515, https://doi.org/10.1002/jbm.a.35500.
- [30] D. Kai, M.P. Prabhakaran, B.Q. Yu Chan, S.S. Liow, S. Ramakrishna, F. Xu, X.J. Loh, Elastic poly(ε-caprolactone)-polydimethylsiloxane copolymer fibers with shape memory effect for bone tissue engineering, Biomed. Mater. 11 (2016), https://doi.org/10.1088/1748-6041/11/1/015007 015007.
- [31] D. Zhang, O.J. George, K.M. Petersen, A.C. Jimenez-Vergara, M.S. Hahn, M.A. Grunlan, A bioactive "self-fitting" shape memory polymer scaffold with potential to treat cranio-maxillo facial bone defects, Acta Biomater. 10 (2014) 4597–4605, https://doi.org/10.1016/J.ACTBIO.2014.07.020.
- [32] R. Xie, J. Hu, X. Guo, F. Ng, T. Qin, Topographical control of preosteoblast culture by shape memory foams, Adv. Eng. Mater. 19 (2017) 1600343, https://doi.org/10.1002/adem.201600343.
- [33] X. Liu, K. Zhao, T. Gong, J. Song, C. Bao, E. Luo, J. Weng, S. Zhou, Delivery of growth factors using a smart porous nanocomposite scaffold to repair a

- mandibular bone defect, Biomacromolecules 15 (2014) 1019–1030, https://doi.org/10.1021/bm401911p.
- [34] H.V. Almeida, B.N. Sathy, İ. Dudurych, C.T. Buckley, F.J. O'Brien, D.J. Kelly, Anisotropic shape-memory alginate scaffolds functionalized with either Type I or Type II collagen for cartilage tissue engineering, Tissue Eng. Part A 23 (2017) 55–68, https://doi.org/10.1089/ten.tea.2016.0055.
- [35] D. Kai, M.J. Tan, M.P. Prabhakaran, B.Q.Y. Chan, S.S. Liow, S. Ramakrishna, X.J. Loh, Biocompatible electrically conductive nanofibers from inorganic-organic shape memory polymers, Colloids Surfaces B Biointerfaces 148 (2016) 557–565, https://doi.org/10.1016/J.COLSURFB.2016.09.035.
- [36] H. Gu, S.W. Lee, S.L. Buffington, J.H. Henderson, D. Ren, On-demand removal of bacterial biofilms via shape memory activation, ACS Appl. Mater. Interfaces. 8 (2016) 21140–21144, https://doi.org/10.1021/acsami.6b06900.
- [37] R.J. Mart, R.D. Osborne, M.M. Stevens, R.V. Ulijn, Peptide-based stimuliresponsive biomaterials, Soft Matter. 2 (2006) 822, https://doi.org/10.1039/ b607706d.
- [38] D.J. Phillips, M. Wilde, F. Greco, M.I. Gibson, Enzymatically triggered, isothermally responsive polymers: reprogramming Poly(oligoethylene glycols) to respond to phosphatase, Biomacromolecules 16 (2015) 3256–3264, https://doi.org/10.1021/acs.biomac.5b00929.
- [39] Y. Wang, J.D. Byrne, M.E. Napier, J.M. DeSimone, Engineering nanomedicines using stimuli-responsive biomaterials, Adv. Drug Deliv. Rev. 64 (2012) 1021– 1030, https://doi.org/10.1016/J.ADDR.2012.01.003.
- [40] Mark A. Rice, Johannah Sanchez-Adams, Kristi S. Anseth, Exogenously triggered, enzymatic degradation of photopolymerized hydrogels with polycaprolactone subunits: experimental observation and modeling of mass loss behavior, Biomacromolecules (2006), https://doi.org/10.1021/BM060086+.
- [41] X. Gu, J. Wu, P.T. Mather, Polyhedral oligomeric silsesquioxane (POSS) suppresses enzymatic degradation of PCL-Based polyurethanes, Biomacromolecules 12 (2011) 3066–3077, https://doi.org/10.1021/bm2006938.
- [42] B. Ding, E. Kimura, T. Sato, S. Fujita, S. Shiratori, Fabrication of blend biodegradable nanofibrous nonwoven mats via multi-jet electrospinning, Polymer (Guildf) 45 (2004) 1895–1902, https://doi.org/10.1016/j. polymer.2004.01.026.
- [43] J.M. Robertson, H. Birjandi Nejad, P.T. Mather, Dual-spun shape memory elastomeric composites, ACS Macro Lett. 4 (2015) 436–440, https://doi.org/ 10.1021/acsmacrolett.5b00106.
- [44] A. Varesano, R.A. Carletto, G. Mazzuchetti, Experimental investigations on the multi-jet electrospinning process, J. Mater. Process. Technol. 209 (2009) 5178– 5185, https://doi.org/10.1016/J.JMATPROTEC.2009.03.003.
- [45] H.B. Nejad, J.M. Robertson, P.T. Mather, Interwoven polymer composites via dual-electrospinning with shape memory and self-healing properties, (n.d.). doi:10.1557/mrc.2015.39.
- [46] H. Birjandi Nejad, J.M. Robertson, P.T. Mather, Interwoven polymer composites via dual-electrospinning with shape memory and self-healing properties, MRS Commun. 5 (2015) 211–221, https://doi.org/10.1557/mrc.2015.39.
- [47] J. Tumbic, A. Romo-Uribe, M. Boden, P.T. Mather, Hot-compacted interwoven webs of biodegradable polymers, Polymer (Guildf). 101 (2016) 127–138, https://doi.org/10.1016/LPOLYMER.2016.08.057.
- [48] X. Luo, P.T. Mather, Design strategies for shape memory polymers, Curr. Opin. Chem. Eng. 2 (2013) 102–110. https://doi.org/10.1016/j.coche.2012.10.006.
- [49] K.A. Burke, P.T. Mather, Evolution of microstructure during shape memory cycling of a main-chain liquid crystalline elastomer, Polymer (Guildf) 54 (2013) 2808–2820, https://doi.org/10.1016/j.polymer.2013.03.049.
- [50] S.J. Busch, G.A. Martin, R.L. Barnhart, R.L. Jackson\$, THE JOURNAL OF BIOLOGICAL CHEMISTRY Heparin Induces the Expression of Hepatic Triglyceride Lipase in a Human Hepatoma (HepG2) Cell Line*, 264 (1989) 9527–9532. http://www.jbc.org/content/264/16/9527.full.pdf (accessed May 10 2017) PMID: 2542313
- [51] S.J. Busch, R.L. Barnhart, G.A. Martin, M.A. Flanagan, R.L. Jackson, Differential regulation of hepatic triglyceride lipase and 3-hydroxy-3-methylglutaryl-CoA reductase gene expression in a human hepatoma cell line, HepG2, J. Biol. Chem. 265 (1990) 22474–22479. PMID (2176219).
- [52] M. Zelzer, L.E. McNamara, D.J. Scurr, M.R. Alexander, M.J. Dalby, R.V. Ulijn, H.G. Neumann, B. Nebe, A. Liebold, G. Steinhoff, J. Rychly, Phosphatase responsive peptide surfaces, J. Mater. Chem. 22 (2012) 12229, https://doi.org/10.1039/c2im31666h
- [53] H.Y. Liu, M. Korc, C.C. Lin, Biomimetic and enzyme-responsive dynamic hydrogels for studying cell-matrix interactions in pancreatic ductal adenocarcinoma, Biomaterials 160 (2018) 24–36, https://doi.org/10.1016/j. biomaterials.2018.01.012.
- [54] D. Roy, J.N. Cambre, B.S. Sumerlin, Future perspectives and recent advances in stimuli-responsive materials, Prog. Polym. Sci. 35 (2010) 278–301, https://doi. org/10.1016/J.PROGPOLYMSCI.2009.10.008.